Wideband chaos generation using a delayed oscillator and a two-dimensional nonlinearity induced by a quadrature phase-shift-keying electro-optic modulator

M. Nourine, Y.K. Chembo, L. Larger

Wideband chaos generation using a delayed oscillator and a two-dimensional nonlinearity induced by a quadrature phase-shift-keying electro-optic modulator

Mourad Nourine, Yanne K. Chembo,* and Laurent Larger

FEMTO-ST Institute (UMR CNRS 6174), Optics Department, P. M. Duffieux, 16 Route du Gray, 25030 Besançon Cedex, France
**Corresponding author: yanne.chembo@femto-st.fr*

We present a new optoelectronic architecture intended for chaotic optical intensity generation. The principle relies on an electro-optic nonlinear delay dynamics, where the nonlinearity originates from an integrated four-wave optical interferometer, involving two independent electro-optic modulation inputs. Consequently, the setup involves both two-dimensional nonlinearity and dual-delay feedback dynamics, which results in enhanced chaos complexity of particular interest in chaos encryption schemes. The generated chaos observed with large feedback gains has a bandwidth ranging from 30 kHz to 13 GHz and is confirmed by numerical simulations of the proposed dynamical model and bifurcation diagram calculation.

Since the first successful demonstrations of optical chaos cryptography [1,2], various architectures have been proposed for the generation of chaotic optical carriers (see [3] and references therein). Chaotic carriers form the entropy source that is encrypting an information-bearing signal. High complexity is a necessary condition when security issues are concerned. This is achieved via a high-dimensional generated chaotic motion. A suitable class of chaotic systems for this purpose is the family of delay-differential equations, that own mathematically an infinite-dimensional phase space. Provided that this infinite dimension is also associated with a strong nonlinearity, a huge number (potentially > 1000) of dimensions may be actually visited by the chaotic attractor. The corresponding motion thereby provides a hyperchaotic encryption masking signal that may spectrally span from a few kilohertz to more than 10 GHz, with spectral features that closely resemble those of a band-limited white noise [4,5]. It has previously been shown that, when properly designed, Ikeda-like delay-differential systems [6] can provide such a hyperchaotic carrier, using, for example, integrated optics lithium niobate ($LiNbO_3$) Mach–Zehnder (MZ) modulators. These standard telecom devices perform unidimensional nonlinearity $\mathcal{F} \equiv \sin^2$, obtained from the transfer function of an electro-optically tunable two-wave interferometer [7]. One issue of such a chaos generator raised in the context of chaos communications and security issues is the design of customized electro-optic devices, in which electro-optically tunable multiple-wave interferometer architectures could lead to enhanced complexity of the obtained chaotic motions. Following this motivation, we propose here to test such a complexity improvement via the use of an unconventional but commercially available electro-optic modulator: a quadrature phase-shift-keying (QPSK) modulator Fig. 1) originally designed for multiple-valued digital modulation format for high-speed optical communications [8]. The QPSK modulator is precisely based on a similar multiple-wave interference electro-optic modulator, with independent modulation inputs, resulting in a two-dimensional (2D) nonlinear modulation transfer function [see Fig. 1(c)]. Moreover, the use of two independent modulation RF electrodes allows one to design a dual-delay feedback Ikeda-like architecture, which is also expected to increase the complexity of the chaotic motion. In the context of chaos communications, an eventual eavesdropper would need to precisely identify many more parameters (the hardware keys) in order to reconstruct the nonlinear dynamics. This reconstruction is so far, to our knowledge, the only proposed cryptanalysis approach that, first, enables the chaos synchronization operation and, then, the decryption, provided the physical parameters are known. Our aim is, therefore, to propose a way to improve the dimensionality of the chaos generator, and at the same to demonstrate the possibility for electro-optic chaos generation [9] involving customized multiple-wave electro-optic modulation. The complete chaos generator is depicted in Fig. 2. In order to derive the dynamical model of such a complex

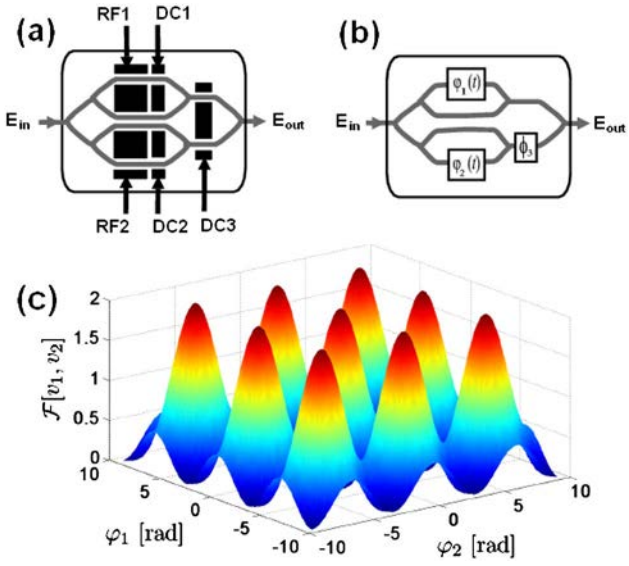

Fig. 1. (Color online) QPSK modulator: (a) device architecture, (b) physical model of the four-wave interferometer, and (c) plot of the 2D nonlinear transfer function.

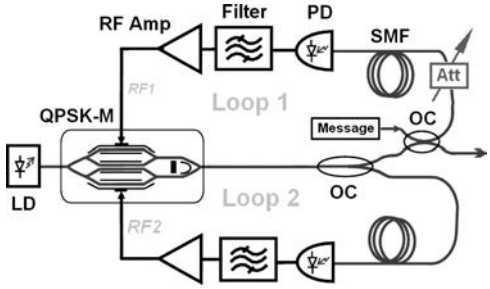

Fig. 2. (Color online) Experimental setup. LD, laser diode; QPSK-M, quadrature phase-shift-keying modulator; RF Amp, radio-frequency amplifier; PD, photodiode; SMF, single-mode fiber; OC, optical coupler; Att, variable attenuator.

nonlinear delay oscillator, we first need to model the nonlinear transformation. The latter is directly performed by the modulation transfer function of the QPSK modulator described in Fig. 1, which is ruling the output intensity modulation with respect to the two electrical RF inputs. As displayed in Fig. 1, the QPSK modulator is an integrated optics (lithium niobate) device. It has five voltage inputs: RF1 and RF2 (half-wave voltages are $V_{\pi\mathrm{RF1,2}}$), which are dedicated to the RF modulation via $v_1(t)$ and $v_2(t)$; and DC1, DC2, and DC3 (half-wave voltages $V_{\pi\mathrm{DC1,2,3}}$), which are dedicated to the bias voltages, V_{B1}, V_{B2}, and V_{B3}, that are used to set the rest point of the 2D multiple-wave interference.

The output power of the QPSK modulator, which is later detected by fast telecom photodiodes, is the time average of the energy interference of the resulting electric field, that is,

$$P_{\mathrm{out}}(t) = \langle |E_{\mathrm{out}}(t)|^2 \rangle = P_{\mathrm{in}} \cdot \mathcal{F}[v_1(t), v_2(t)]. \qquad (1)$$

The input electric field can be written as $E_{\mathrm{in}}(t) = \sqrt{P_{\mathrm{in}}} \exp(i\omega_0 t)$, where P_{in} is the optical power of the CW laser beam at the input of the QPSK modulator, while $\omega_0 = 2\pi c/\lambda_0$ is the angular frequency of the laser source (central wavelength $\lambda_0 \simeq 1.55\,\mu$m), c being the velocity of light in vacuum. The function $\mathcal{F}[v_1, v_2]$ is the normalized 2D nonlinear transformation performed by the QPSK modulator with respect to its RF input voltages v_1 and v_2. Considering the interferences related to the various optical paths depicted schematically in Fig. 1, the output electric field $E_{\mathrm{out}}(t)$ of the QPSK modulator is given by

$$E_{\mathrm{out}}(t) = \frac{E_{\mathrm{in}}(t)}{2} \times \{1 + e^{i\varphi_1(t)} + [1 + e^{i\varphi_2(t)}]e^{i\phi_3}\}, \qquad (2)$$

where $\phi_k = \pi V_{Bk}/(2V_{\pi\mathrm{DC}k})$ (with $k = 1, 2, 3$) and $\varphi_k(t) = \pi v_k(t)/(2V_{\pi\mathrm{RF}k}) + \phi_k$ (with $k = 1, 2$) are the various electro-optically induced phase shifts associated to the different optical paths. After some straightforward algebra, it can be deduced that the 2D nonlinear transfer function of the QPSK modulator is

$$\begin{aligned}\mathcal{F}[v_1(t), v_2(t)] = \frac{1}{2}\{&\cos^2\phi_3 + \cos^2[\varphi_1 - \varphi_2 - \phi_3] \\ &+ 2\cos\phi_3 \cos[\varphi_1 - \varphi_2 - \phi_3] \\ &\times \cos[\varphi_1 + \varphi_2]\}, \end{aligned} \qquad (3)$$

which corresponds to a periodic bidimensional landscape as can be seen in Fig. 1(c). Here lies one of the specific interests of this 2D transfer function: it depends on more parameters than a conventional MZ modulator, and it can be, in principle, designed by any kind of customized multiple-wave integrated optics interferometer. Moreover, the two modulation branches of the QPSK modulator allow for a dual-loop configuration, thereby adding another degree of complexity through the two corresponding time delays.

Once this QPSK modulator is integrated in a delayed opto-electronic oscillator, as depicted in Fig. 2, the whole system consists of (i) the QPSK modulator described above, with $V_{\pi\mathrm{RF1}} = 5.84\,\mathrm{V}$ and $V_{\pi\mathrm{RF2}} = 6.08\,\mathrm{V}$, (ii) two fiber delay lines performing time delays equal to $T_1 = 61\,\mathrm{ns}$ and $T_2 = 60\,\mathrm{ns}$, (iii) two fast photodiodes with a conversion factor of $S_{1,2} = 2\,\mathrm{V/mW}$, (iv) two RF drivers with gains $G_{1,2}$ of 18 dB, (v) two band-limiting bandpass filters with bandwidths ranging from $f_{L1} = 50\,\mathrm{kHz}$ to $f_{H1} = 13\,\mathrm{GHz}$ for the first loop, and from $f_{L2} = 30\,\mathrm{kHz}$ to $f_{H2} = 13\,\mathrm{GHz}$ for the second, (vi) attenuation factors η_1 and η_2, which gather the optical and electrical losses in each loop, and (vii) a 1×2 optical coupler that enables us to feed a fraction of the QPSK modulator optical output into each loop (a 2×2 coupler could also be useful for the message insertion).

The dynamics of the microwave oscillation can be described in terms of the dimensionless variable $x_k(t) = \pi v_k(t)/2V_{\pi\mathrm{RF}k} = \varphi_k(t) - \phi_k$ (with $k = 1, 2$). The normalized dynamics is thus ruled by the following integro-differential nonlinear delayed equation:

$$x_k + \tau_k \frac{dx_k}{dt} + \frac{1}{\theta_k}\int_{t_0}^{t} x_k(\xi)\mathrm{d}\xi = \beta_k \mathcal{F}[x_1(t - T_k), x_2(t - T_k)], \qquad (4)$$

where $\beta_k = \pi\eta_k S_k G_k P/2V_{\pi\mathrm{RF}k}$ is the normalized loop gain, while $\tau_k = 1/(2\pi f_{Hk})$ and $\theta_k = 1/(2\pi f_{Lk})$ are the two characteristic time scales of the bandpass filter. Equation (4), therefore, represents a set of two coupled second-order differential equations.

This model has been numerically integrated using the predictor–corrector algorithm. A bifurcation diagram has been plotted to illustrate the qualitative dynamical behavior of the system as a function of the feedback gains. For the sake of simplicity, we have focused on the dynamics of only the first loop, when its gain β_1 is varied using the variable attenuator, while β_2 is kept constant. In Fig. 3(a), it is experimentally observed that, as the gain is increased, the system undergoes a cascade of bifurcations until it reaches the state of fully developed chaos. This kind of behavior is well known in delay systems, and it has earlier been shown to follow a typical route to chaos through a primary Hopf bifurcation, eventually followed by other more exotic bifurcations, resulting, for example, in the occurrence of chaotic breathers [5], but finally leading rapidly to the desired chaotic motions for high enough feedback strength. This phenomenology has been recovered through numerical simulations in Fig. 3(b). We have also numerically computed the entropy of the chaotic signal using the formula $\Omega = -\sum_{i=1}^{N} p_i \log_2 p_i$, where N is the number of motion

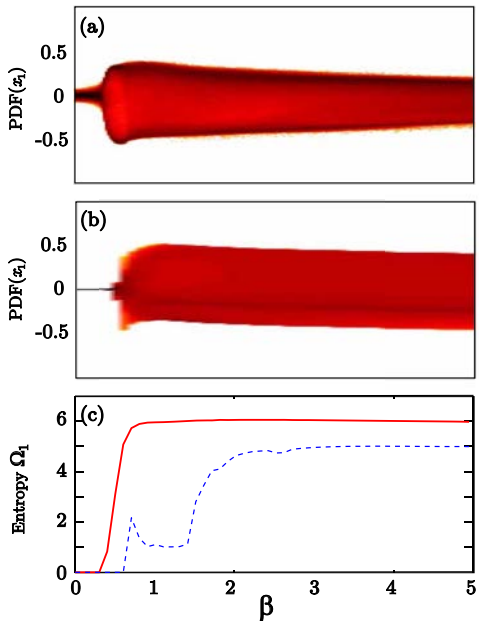

Fig. 3. (Color online) Bifurcation diagrams [(a) experiment and (b) numerics] of the probability density function (PDF) of the solution trajectory $x_1(t)$, as β_1 is increased, with $\phi_1 = 1.59\,\text{rad}$, $\phi_2 = 0.39\,\text{rad}$, $\phi_3 = -0.11\,\text{rad}$, and $\beta_2 = 1.1$. (c) Corresponding entropy Ω_1 (numerics; dashed curve, single loop entropy, i.e., for $\beta_2 = 0$).

amplitude bins, while p_i is the probability density associated to the ith bin. It appears in Fig. 3(c) that, owing to the QPSK 2D nonlinearity, the entropy saturates very rapidly (as soon as $\beta \sim 0.7$) and much more abruptly compared to standard Ikeda dynamics (single loop entropy evolution, dashed curve).

The experimental time trace of the chaotic RF variable is also displayed in Fig. 4(a), along with its power spectrum [Fig. 4(b)]. This output variable is strongly high dimensional, its dimension being roughly of the order of $T_1/\tau_1 \sim 5000$ [10]. It is particularly noteworthy that the spectrum of the chaotic dynamics spans at up to 13 GHz, and that there are no spectral signatures arising from cavity resonances or from relaxation oscillations (see the zoomed insets, where no delay modulation at $1/T \simeq 16\,\text{MHz}$ can be observed).

In conclusion, we have proposed a new architecture for the generation of wideband chaos, based on the 2D nonlinearity of a QPSK modulator. We have shown how this integrated component increases the dynamical complexity, and we have proposed a model to investigate its various dynamical properties. Further investigations will focus on the integration of this QPSK-based

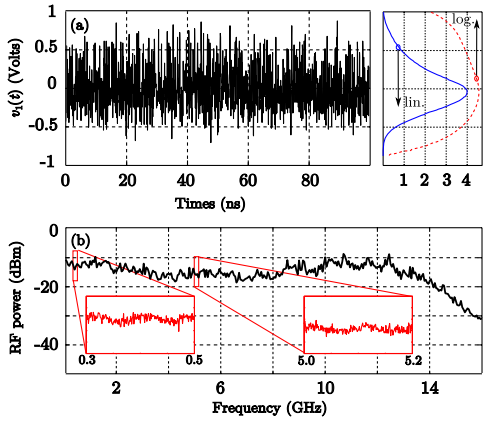

Fig. 4. (Color online) (a) Experimental time series for $\beta_1 = 5.0$, and amplitude probability distribution (right plot; linear, lower axis; log scale, upper axis) [other parameters identical as in Fig. 3(a)]. (b) Corresponding RF power density spectrum (1 MHz resolution).

oscillator in an emitter–receiver configuration, in view of chaos communications [3,7,11]. However, beyond cryptographic applications, the statistical properties of this hyperchaotic signal can also be used for other applications, such as the ultrafast (>10 Gsamples/s) generation of quasi-random Gaussian distributed numbers, or as a deterministic probe signal for ultrawideband radar systems.

References

1. J. P. Goedgebuer, L. Larger, and H. Porte, Phys. Rev. Lett. **80**, 2249 (1998).
2. G. D. Van Wiggeren and R. Roy, Science **279**, 1198 (1998).
3. A. Argyris, D. Syvridis, L. Larger, V. Annovazzi-Lodi, P. Colet, I. Fischer, J. Garcia-Ojalvo, C. R. Mirasso, L. Pesquera, and K. A. Shore, Nature **437**, 343 (2005).
4. K. E. Callan, L. Illing, Z. Gao, D. J. Gauthier, and E. Schöll, Phys. Rev. Lett. **104**, 113901 (2010).
5. Y. C. Kouomou, P. Colet, L. Larger, and N. Gastaud, Phys. Rev. Lett. **95**, 203903 (2005).
6. K. Ikeda, Opt. Commun. **30**, 257 (1979).
7. J.-P. Goedgebuer, P. Levy, L. Larger, C.-C. Chen, and W. T. Rhodes, IEEE J. Quantum Electron. **38**, 1178 (2002).
8. T. Pfau, S. Hoffmann, R. Peveling, S. Ibrahim, O. Adamczyk, M. Porrmann, S. Bhandare, R. Noé, and Y. Achiam, Electron. Lett. **42**, 1175 (2006).
9. M. Nourine, M. Peil, and L. Larger, in *C. R. Rencontres du Non Linéaire* (2009), Vol. 12, 149.
10. J. D. Farmer, Physica D **4**, 366 (1982).
11. Y. C. Kouomou, P. Colet, L. Larger, and N. Gastaud, IEEE J. Quantum Electron. **41**, 156 (2005).